Semi-Annual Report Submitted to the
National Aeronautics and Space Administration

For January - June, 2000

Contract Number: NAS5-31370

Land Surface Temperature Measurements from EOS MODIS Data

MODIS Team Member
PRINCIPAL INVESTIGATOR

ZHENGMING WAN

P.I.'s Address:

Institute for Computational Earth System Science
University of California
Santa Barbara, CA 93106-3060

phone : (805) 893-4541
Fax no: (805) 893-2578
E-mail: wan@icess.ucsb.edu

Land Surface Temperature Measurements from EOS MODIS Data

Semi-Annual Report for July - December, 1999

Zhengming Wan

Abstract

The quality of early MODIS TIR channel data was evaluated over some special lake sites which were apparently covered by melting snow/ice and surrounded with snow covers. The MODIS data over such a lake in Kamchatka, Russia on 13 April 2000 indicate that the ninth channel in bands 21 and 24, and the fourth channel in band 22 are very noisy, and that the maximum difference and standard deviation of band 31 brightness temperatures in a sub-area of 10 by 5 pixels are 0.24K and 0.04K, respectively. After skipping the noisy channels, the standard deviations in other bands but band 21 range from 0.10 to 0.68K, indicating satisfactory signal-to-noise ratios of the MODIS TIR data. Modifications were made in the product generation executive code PGE16 for the daily MODIS Land-surface Temperature (LST) product to avoid the effects of the noisy channels. A vicarious calibration field campaign was conducted in Bolivia during May 26 and June 17, 2000. The calculated band brightness temperatures based on lake surface temperatures measured by multiple IR radiometers and thermistors deployed in the high-elevation Lake Titicaca (3841m above sea level) and the atmospheric temperature and water vapor profiles measured by radiosondes launched by the lakeshore are well matched the MODIS TIR data produced by the new Level-1B code (version 2.4.2). On a perfect clear-sky day, 15 June 2000, all in-situ measurements were made successfully, atmospheric temperature and water vapor profiles were measured up to 22km above sea level. The comparison between the MODIS TIR data and the calculated values based on in-situ measurement data indicates that the absolute radiometric accuracies specified for the MODIS bands above 3 μm are achieved in 10 out of all 16 bands and that the calibration error in the high temperature band 21 for fire detection is approximately 1-2K. The radiometric calibration error is less than 0.4% in bands 31 and 32. In-situ measurements were also made to validate the MODIS LST product in two validation field campaigns in the areas of Mono Lake, California, and Railroad Valley, Nevada, one in late March to early April, another in late July to early August.

Recently Published Papers

X. Ma, Z. Wan, C. C. Moeller, W. P. Menzel, L. E. Gumley, and Y. Zhang, "Retrieval of geophysical parameters from Moderate Resolution Imaging Spectroradiometer thermal infrared data: evaluation of a two-step physical algorithm", Applied Optics, Vol. 39, No. 20, pp. 3537-3550, 2000.

1. Quality Evaluation of the Early MODIS TIR Channel Data

In order to evaluate the quality of early MODIS TIR channel data we found some special lake sites which were apparently covered by melting snow/ice and surrounded with snow covers. If the science data snowcover in the daily MODIS Snowcover product is given 200 for a pixel, this pixel is believed as 100% snow cover. If this value is 100, there may be at least two possible explanations. The first one is that approximately a half of the pixel is covered by snow and another half is one type or a mixture of land covers but not snow, for example forest. It is hard for us to believe this explanation for large lakes because it seems impossible that all of a large number of pixels in a lake are covered by snow and water/ice half by half. The second explanation is that the snow cover is in the status of melting so that the signal received by the MODIS visible channels is only about a half of the signal of typical snow covers. We believe that the second explanation is more suitable for large lakes if all pixels within a significant portion of a lake have snowcover value 100 and a large number of pixels surrounding the lake have snowcover value 200. We found this situation in granule A2000104.0055 (April 14) over a lake in Kamchatka, Russia, granule A2000103.0335 (April 13) over Hulun Nur (lake), China, granule A2000115.1710 (April 24) over Lake Nipigon, Canada, granule A2000128.0505 (May 7) over Hovsgol Lake, Mongolia. A major advantage of such scenes is that the surface temperature of melting snow/ice is around a fixed value, i.e., 273.15K. Therefore, the spatial variation in the MODIS TIR data is caused only by the spatial variations in the surface reflectance and emissivity, and the atmospheric conditions. Because both snow and water have high emissivities (around 0.99) in band 31 and the atmospheric effect in band 31 is relatively small so that the spatial variation caused by the changes in atmospheric conditions will be minimum in band 31. We calculated the maximum, minimum, average and standard variation of brightness temperatures in all TIR channels over a sub-area of at least 10 by 5 pixels within the above lakes and found the best results (minimum values of the maximum temperature difference ΔT_b and the standard deviation δT_b in the granule A2000104.0055 over the lake in Kamchatka, Russia. These results are given in Table I. In the upper portion, the ΔT_b and δT_b values are given for bands 29-36 when all channels in these bands are included in the analysis. In band 31, the maximum temperature difference is 0.24K, and the standard deviation is 0.04K. If we assume that half of the maximum temperature difference is due to the variations in surface and atmospheric conditions, the noise equivalent temperature difference (NEΔT) will be around 0.1K in band 31. Because the effects of spatial variations in surface and atmospheric conditions on ΔT_b and δT_b are larger in other bands, it is not easy to estimate their NEΔT values. The ΔT_b and δT_b values for bands 20-25 and 27-28 are given in the middle and lower portions of Table I. In the middle portion, all channels are considered in the calculations. The ΔT_b and δT_b values in bands 21, 22, and 24 are more than 10 times larger than those values in other bands. After skipping the noisy ninth channel in bands 21 and 24, and the fourth channel in band 22, the ΔT_b and δT_b values are much smaller as show in the lower portion. As shown in section 3, the spatial variations in the atmospheric temperature and water vapor profiles have significant effects on the TIR signals received by satellite TIR sensors. The reflected solar

radiation in band 20 will change significantly even for a small variation in the surface reflectance. Therefore, it seems reasonable to assume that a variation in the reflected solar radiation accounts for major portions of the ΔT_b and δT_b values in band 20, and that the spatial variation in the atmospheric conditions accounts for major portions in all bands. After considering these two facts, the δT_b values in the upper and lower portions may be reduced by a factor of 2 or 3 in all bands, and another factor of 2 or 3 in band 20, then the noise-equivalent temperature difference NEΔT specified in page 10 of the document "Specification for the Moderate-resolution Imaging Spectrometer - NADIR (MODIS-N)" (draft Ver 2.2, 1/29/92, no. 422-20-02, October 5, 1990, Goddard Space Flight Center) may be reached or is nearly reached in all channels except the three noisy channels. In this document there is no specification for the fire detecting band 21. We assumed a specification of 2K for band 21 in Table I.

2. Update of the MODIS LST Product Generation Executive Code (PGE16)

The noisy fourth channel in band 22 and ninth channel in band 24 will affect the MODIS LST product directly and indirectly. First of all, these two bands are used in the day/night LST algorithm (Wan and Li 1997) to produce the daily 5km LST product. Secondly, the noisy fourth channel in band 22 also affects the generalized split-window LST algorithm (Wan and Dozier, 1996) to produce the daily 1km LST product through the cloudmask product (MOD35) as input to the PGE16.

In the MODIS cloudmask algorithm, band 22 is used in the 4-11 micron test to determine the cloudyness of a pixel. Because of this, the noisy fourth channel in band 22 produced quite a lot of (cloud) strips in the cloudmask product. This phenomenon propagates into the MODIS LST product.

To avoid the problems caused by the noisy channels, we modified the PGE16 in two ways. In the day/night LST algorithm, the fourth and ninth channels of MODIS L1B data are skipped so that 20 pixels instead of 25 pixels will be used to get the averaged brightness temperatures in bands 20, 22-23, 29, 31-33. In the generalized split-window LST algorithm, the cloudmask in all fourth channels of the scan cubes (one scan cub contains ten channels in each band) is refined with the neighboring pixels in the third and fifth channels. If both the neighboring pixels in the third and fifth channels are clear-sky pixels at a 99% confidence, the pixel in the fourth channel will be treated as clear-sky pixel for the LST retrieval.

3. Vicarious Calibration of the MODIS TIR Channel Data

3.1. Advantages of using Lake Titicaca, Bolivia, as a vicarious calibration site

According to the experience gained in our field campaigns for the validation MAS/MODIS LST algorithms and products (Wan and Dozier, 1996; Wan and Li 1997; Snyder et al., 1997a; Wan et al., 1999), the major sources of uncertainties in the validation of TIR products include: (a) the uncertainties in atmospheric water vapor and temperature profiles, (b) the uncertainties in the atmospheric molecular absorption coefficients that are used in the atmospheric transmission and radiance calculations based on measured

atmospheric profiles, (c) the spatial variations in surface temperature and emissivity within the TIR scene.

The radiosonde measurement usually takes more than one hour for a set of atmospheric temperature and water vapor profiles. During this time, the radiosonde balloon may shift 20-50km in the horizontal direction in windy conditions. Considering the high temporal and spatial variations in the atmospheric status (especially water vapor) and the errors in radiosonde data, the differences between the measured temperature and water vapor profiles and the actual profiles for the real satellite observation may be up to several degree K and 30%, respectively.

It is easily understandable to use clear-sky oceans or lakes as the validation sites for the absolute calibration of TIR radiance because the flat water surface (under low wind conditions) is the only Earth scene which emissivity and its polarization can be accurately calculated (Born and Wolfe, 1980) from refractive index of water (Hale and Querry, 1973). For example, the performance of the MODIS Airborne Simulator (MAS) has been validated in the field campaigns conducted in the Gulf of Mexico (King et al., 1996) and at the Mono Lake (Wan et al., 1999). Although the emissivities of snow and ice are comparable to water emissivity in the TIR range of interest, but they change with particle size, surface roughness, and the presence of meltwater so that it is difficult to know the exact values of the spectral emissivities of snow and ice in the field to the accuracy required for the validation of MODIS absolute radiance in the TIR region.

Smith et al. (1996) showed that the sea surface temperature was measured to an accuracy believed to be better than 0.1 °C with the Atmospheric Emitted Radiance Interferometer (AERI) over the Gulf of Mexico during a 5-day oceanographic cruise in January 1995 and that for microwindows, the narrow windows between absorption lines where the atmospheric effects are small, observed with high spectral resolution instruments such as ER-2 HIS (High Resolution Interferometer Sounder), the uncertainty in the calculated top-of-the atmosphere (TOA) radiances based on measured atmospheric temperature and water vapor profile is weakly dependent on the accuracy of the atmospheric temperature and water vapor profile. However, for other narrow bands of HIS and for moderate resolution TIR channels of MODIS this uncertainty may be strongly dependent on the accuracy of the atmospheric temperature and water vapor profile, and on the accuracy of the empirical water vapor continuum absorption (Clough et al., 1986) used in atmospheric radiative transfer calculations. Therefore, the accuracy and representativeness of measured atmospheric profiles are crucial for the success of vicarious calibration activities.

Lake Titicaca is an ideal validation site for the TIR absolute radiances because of the following reasons: (a) its is a high elevation (3841m above sea level) lake located in a large plateau; (b) it has a large size of open water surface (8,100 km^2); (c) there are only very light boating activities on the lake in the winter; (d) the spatial variation in the lake-surface temperature is often very small (the maximum difference in brightness temperatures of MODIS band 31 in a sub-area larger than 30 by 30km is not larger than 0.5K, for example, in the MODIS data on May 24, June 3, June 15, 21 and 23, 2000); (e) over the lake area and

its surroundings the atmosphere is dry in the winter; (f) there is a high chance of clear-sky days in the winter and high visibilities (low aerosol densities) in clear-sky days. Figure 1 is the black-white copy of a MODIS color composite image over Bolivia on June 15, 2000, with brightness temperatures in band 20, 29, and 31 as RGB. The uniformly grey area in the upper portion is Lake Titicaca. The dark area by the lower right corner is Uyuni Salt Flats.

3.2. Results from our Lake Titicaca field campaign in May/June 2000

We conducted a field campaign in Bolivia during May 26 and June 17, 2000. Two sub-groups made in-situ measurements over the high-elevation Uyuni Salt Flats and Lake Titicaca sites from the beginning. After ten days, the two groups all worked at the Lake Titicaca site and radiosonde balloons were launched in all clear-sky days. Lake surface temperature measurements were made over a wide open water area of the small portion of Lake Titicaca by Huatajata, La Paz, Bolivia. The dimension of the open water area is 35km in the E-W direction and 15km in the S-N direction. Eight temporary buoys (each made of a basketball, rope, and rocks) were deployed during the field campaign. One thermistor-datalogger system was connected to each buoy and the thermistor was placed about 1cm beneath the water surface. Four-five IR radiometers (IR thermometers from Heitronics) were also connected to the buoys in the middle. They were all far away from the lakeshore at a distance of larger than 3km. Four IR radiometers were placed at the corners of a parallelogram, about 1km long in the N-S side and 1.5km long in the E-W side. Another one was placed in the middle buoy. The orientation of the parallelogram was almost parallel to the daytime Terra orbit. The latitude and longitude values of buoy locations for the radiometers are given in Figure 2. Each IR radiometer was supported by a floating system. The floating system was built with plastic tubes (1" diameter and 60" long each) and basketballs. Four plastic tubes consist a rectangular. Two semi circles of the plastic tubes joined together were connected to the diagonal corners. Four basketball were connected to the corners to provide the floating capability of the system. The IR radiometer mounted on the floating system looks down at a height of 75cm above the water surface with a instant-field-of-view (IFOV) of 32cm in diameter. The advantages of this floating system include its light weight for easy transportation by a small boat, small cross sections in the water so that its disturbance on the water surface is minimum and small cross sections in the air so that its effect on the radiometric measurement is negligible.

We made 13 sets of in-situ measurements covering the daytime or nighttime Terra overpasses under clear-sky conditions, which include May 29 day and night, May 31 day and night, June 3 day and night, June 4 day and night, June 5 day, June 12 night, June 13 day, June 14 night, and June 15 day. After comparing all the cases, we found that the June 15 daytime is the best because of the following reasons: clear atmosphere all over the sky since the evening of the previous day, wind speed of 0.2-0.5m/s before, during, and after the Terra overpass, successful in-situ measurements of the lake surface temperature and balloon release.

Besides the continuous measurements of the lake surface temperatures by five IR radiometers at the buoy positions, the spatial distribution of lake surface temperature was also measured by an IR radiometer which was placed in the front of a moving boat. The radiometer was about 2m away from the boat edge so that it can measure the lake surface temperature before the surface was disturbed by the waves caused by boat's movement. As shown in Fig. 2(a), this IR radiometer gave the lake surface temperature on the way from our base at the lakeshore in Huatajata to the buoy positions listed in Fig. 2(b-f). The last radiometer was deployed around 9:42 local time. Then the boat moved away to the west by 1.5km so that the area covered by buoys would not be disturbed by boating during the Terra overpass. Note that the measurement of the IR radiometers was not affected by the downward atmospheric radiation reflected by the water surface given the extremely dry atmospheric condition. We should add 0.75K on the lake surface temperature measured by the IR radiometers for the correction of the effect of water surface emissivity in the 10-13μm spectral window of the IR radiometer. After this correction, the difference between the lake surface kinetic temperatures measured by the IR radiometers and bulk temperatures measured by thermistors about 1cm beneath the water surface is around 1.25K.

A radiosonde balloon was lifted to 22km above sea level under the weak wind condition gave us a chance to measure the atmospheric temperature and water vapor profiles up to the middle stratosphere. As shown in Fig. 3(a), the measured atmospheric temperature profile is very close to the averaged tropical atmospheric profile. There are only small differences at elevation levels from 15km to 22km. Therefore, it is reasonable to use the averaged tropical atmospheric profile at levels above 22km. The measured water vapor profile shown in Fig. 3(b) gives a column water vapor of 0.286cm, indicating a very dry atmospheric condition.

The MODIS Geolocation product, MOD03.A2000167.1525.002.2000183215414.hdf, gives viewing zenith angle 34.4° from the west, solar zenith angle 43.0° and azimuth angle 23.6°, and the earth view time 15:26:20 UTC for the pixels around our buoy positions at Lake Titicaca on 15 June 2000.

Based on the lake surface temperature measured by IR radiometers and the correction for the emissivity effect, the surface kinetic temperature is 284.79K at the MODIS observation time. Combined with the measured atmospheric temperature and water vapor profiles, we can calculate the spectral radiance at the top-of-the atmosphere (TOA) at the MODIS viewing angle. We used the state-of-art atmospheric radiative transfer model MODTRAN4.0 (berk et al., 1999), the newly released version of MODTRAN code to calculate the TOA radiance. The column ozone calculated from the atmospheric profile is 0.266 ATM CM (equivalent to 266 Dobson Units). The EP/TOMS total ozone map on June 15, 2000 gives a range of 250-275 DU for the Lake Titicaca region (thanks to the NASA TOMS web page http://toms.gsfc.nasa.gov). The calculated spectral atmospheric transmission is given in Figure 4, showing the atmospheric transmission at viewing angle 34.3° greater than 0.95 for most of the 3.7-4.1 and 8-13μm atmospheric windows. Because of the low surface wind speed (less than 0.5m/s), there were only small ripples over the

lake surface so that the lake surface is basically flat. The MODIS viewing angle (34.4° from the west) was far away from the specular reflecting direction of the incident solar beam at zenith angle 43.0° and azimuth angle 23.6°. Therefore, the solar radiation was not included in our radiative transfer calculations. The water surface is assumed as a Lambertian surface for the reflection of the downward atmospheric radiation in the TIR region for simplicity.

With the MODIS relative spectral response functions we can calculate the band brightness temperatures (T_b) for all MODIS TIR bands. In Table II, we compared the calculated T_b values (in column 2) with the T_b values (in column 3) given by the MODIS L1B data generated by the new Level-1B code (version 2.4.2), i.e., MOD021KM.A2000167.1525.002.2000203075713.hdf, giving their differences in column 4. The standard deviation δT_b values shown in Table I are also given in column 6. The δT_b values required to achieve the radiometric accuracies 1% and 2% specified in section 3.4.5.2 Absolute Radiometric Accuracy of the document no. 422-20-02 are given in the last two columns. This document says that "At any other radiance between $0.3L_{typical}$ and $0.9L_{max}$ the absolute accuracy of the radiance shall not exceed the values in Table 3.4.5.2 (1%) by more than 1%".

Table II shows that 10 of the 16 MODIS TIR bands (i.e., bands 21-23, 28-29, and 31-35) meet or nearly meet the requirements for radiometric accuracy 1%, band 30 meets the requirement for radiometric accuracy 2%, four bands (i.e., bands 24-25, 27, and 36) cannot meet the requirements for the absolute radiometric accuracy 2%. For band 20, the δT_b value 0.63K corresponds to radiometric accuracy 3%. As mentioned above, we did not include the solar radiation in the radiative transfer calculations. This δT_b value may be reduced slightly if the solar radiation and an accurate surface reflective model are included in the radiative transfer calculations.

There was also no cloud during the Terra nighttime overpass on June 14, 2000. We also launched a radiosonde balloon and measured the lake surface temperature with IR radiometers. The comparison between calculated T_b and MODIS T_b values from L1B data in the granule MOD021KM.A2000167.0255 is shown in column 5 with δT_b values in bands 20, 29, and 31 only because the atmospheric effects in these three bands are minimal. The δT_b value 0.26K in band 20 corresponds to 1.25% of the radiometric accuracy. But we do not consider the measurement data sets on June 14 night as optimal for the purpose of vicarious calibration because of the following reasons. The MODIS viewing zenith angle is 56.9°. The surface wind speed was 2-4m/s and the balloon was only lifted up to 16km above sea level.

3.3. Sensitivity and error analysis

We made a series of atmospheric radiative transfer simulations for the changes of atmospheric and surface conditions and summarized the results in Tanle III. Considering the measured atmospheric temperature and water vapor profiles and the environmental conditions for the measurement at Lake Titicaca on June 15 (the wind speed and the openness of the lake and its surroundings), we assume the uncertainties in

atmospheric temperature, water vapor, CO_2 and ozone densities as 0.5K, 10%, 10ppm, and -6%, respectively. The change in atmospheric temperature has significant effects on all but five bands (band 20, 22-23, and 31-32). The change in water vapor has significant effects on bands 27-28 only. The change in ozone has a significant effect only on band 30. For the effect of surface bi-directional reflectance distribution function (BRDF), we calculated the difference in T_b in conditions of a Lambertian surface and a specular surface. This effect is small in all but three bands (i.e., larger effects in bands 33-35).

We give the detailed error analysis of the measured lake surface temperature as follows. The IR radiometers are routinely calibrated with blackbodies. Its accuracy is better than 0.2K. As shown in Fig. 2, the spatial variation in the lake surface temperature measured by the five IR radiometers was up to 0.8K at the time of Terra overpass. This is consistent with the spatial pattern of the T_b values from the MODIS L1B data. The average and standard deviation of the measured lake surface temperature are 284.79K and 0.29K, respectively. The uncertainty in the averaged lake surface temperature is less than 0.15K. The root sum squares (RSS) of 0.2K and 0.15K is 0.25K, which is the δT_s value listed in column 8 of Table III.

The total RSS values are given in column 9 for all bands but band 21. Comparing them to the δT_b values required to meet the radiometric accuracies 1% and 2% given in the last two columns, we can get the following insights: 1) the radiometric accuracy 1% may be achieved or nearly achieved in 10 bands (bands 21, 22-23, 29, 31-36; 2) bands 31-32 may achieve an radiometric accuracy of 0.4%, and band 29 may achieve 0.53%; 3) the radiometric accuracy 2% may be achieved in bands 24-25, 28, and 30; 4) it is difficult to achieve the radiometric accuracy 2% in band 27.

The above sensitivity and error analysis supports the findings in the last section for the calibration accuracies of MODIS TIR bands based on our first vicarious calibration field campaign over Lake Titicaca, Bolivia, in May/June 2000.

So far we have not dealt with the polarization explicitly. We used the unpolarized water emissivity, which is the average of polarization emissivities, in atmospheric radiative transfer simulations. The unpolarized reflectance (averaged from polarization reflectances) of the MODIS scan mirror is used in the MODIS L1B code. But infrared radiances from water surface become partially polarized at oblique viewing angles through both emission and reflection (Shaw, 1999). At viewing angle $34.3°$, the p-polarization emissivity (ε_p) of water is larger than the s-polarization emissivity (ε_s) up to 0.05 in the 3-14.5 μm spectral region, and up to 0.02 in the 11-12μm region. The viewing angle $34.3°$ corresponds to an incident angle around $50°$ on the MODIS scan mirror. According to the witness sample measurement data of the MODIS scan mirror, the s-polarization reflectance (R_s) is larger than the p-polarization reflectance (R_p) up to 0.1 at incident angle $50°$. The difference reduces to 0.05 in the 11-12μm region, and to 0.02 in the 3.5-7μm region. Because ε_p is larger than ε_s and R_p is less than R_s, in the first order of approximation, the total TIR signature received by the MODIS sensor is proportional to $0.5(\varepsilon_p \times R_p + \varepsilon_s \times R_s) = 0.5[(\varepsilon + 0.5\times\delta\varepsilon)(R - 0.5\times\delta R) + (\varepsilon - 0.5\times\delta\varepsilon)(R + 0.5\times\delta R)] = \varepsilon R[1 - \delta\varepsilon\,\delta R/(4\varepsilon R)] \approx \varepsilon R(1 - 0.0014)$ when

$\delta\varepsilon = 0.05$ and $\delta R = 0.1$, where $\varepsilon = 0.5(\varepsilon_p + \varepsilon_s)$, $\delta\varepsilon = (\varepsilon_p - \varepsilon_s)$, $R = 0.5(R_s + R_p)$, and $\delta R = (R_s - R_p)$. Therefore, considering the polarizations in water emissivity and mirror reflectance will not make a significant difference in the comparison between calculated radiances and the MODIS radiances. More work will be done for the polarization analysis after the polarization reflectance data of the MODIS scan mirror are validated and available.

4. Field Campaigns for the Validation of MODIS LST Products

We conducted two field campaigns to validate the MODIS LST Product, one in the area of Mono Lake, California, in late March to early April, another in the areas of Mono Lake, California, and Railroad Valley, Nevada, in late July to early August. In-situ measurements of the land-surface temperature were made with IR radiometers and spectrometers. We are waiting for the MODIS L1B data produced by the new Level-1B code (version 2.4.2), and other products (MOD07, MOD35, and MOD10_L2) based on the new L1B data. These data will be used as input data for the MODIS LST algorithm to generate MODIS LST products.

Acknowledgment

The following scientists participated in the Bolivia field campaign: Zhengming Wan, Yulin Zhang, and Zhao-liang Li of the Institute for Computational Earth System Science (ICESS), University of California at Santa Barbara (UCSB), Arnaud Yves of the French Institute of Research and Development (IRD), La Paz, Bolivia, Roland Bosseno and Jean Francois Hanocq of INRA - Bioclimatology, France. Ruibo Wang and Xialin Ma of ICESS, UCSB, participated in the field campaigns conducted in California and Nevada. The MODIS data were generated by the Goddard DAAC and MODAPS under supports of MODIS MCST and SDDT. We also used the EP/TOMS total ozone image of 15 June 2000 from the NASA TOMS web page (http://toms.gsfc.nasa.gov).

REFERENCES

Berk, A., G. P. Anderson, L. S. Bernstein, P. K. Acharya, H. Dothe, M. W. Matthew, S. M. Adler-Golden, J. H. Chetwynd, Jr., S. C. Richtmeier, B. Pukall, C. L. Allred, L. S. Jeong, and M. L. Hoke, ‘‘MODTRAN4 radiative transfer modeling for atmospheric correction,’’ *Optical Spectroscopic Techniques and Instrumentation for Atmospheric and Space Research III*, vol. 3756, SPIE, 1999.

Born, M. and E. Wolfe, *Principles of Optics, 6th ed.,* New York: Pergamon Press, 1980.

Clough, S. E., F. X. Kneizys, E. P. Shettle, and G. P. Anderson, ‘‘Atmospheric radiance and transmission: FASCOD2,’’ in *Proc. of the Sixth Conference on Atmospheric Radiation, Williamsburg, VA*, pp. 141-144, Boston, MA: American Meteorological Society, 1986.

Hale, G. M. and M. R. Querry, ‘‘Optical constants of water in the 200-nm to 200-µm wavelength region,’’ *Appl. Optics*, vol. 12, no. 3, pp. 555-641, 1973.

King, M. D., W. P. Menzel, P. S. Grant, J. S. Myers, G. T. Arnold, S. E. Platnick, L. E. Gumley, S. C. Tsay, C. C. Moeller, M. Fitzgerald, K. S. Brown, and F. G. Osterwisch, ‘‘Airborne scanning spectrometer for remote sensing of cloud, aerosol, water vapor and surface properties ,’’ *J. Atmos. Ocean. Technol.*, vol. 13, pp. 777-794, 1996.

Shaw, J. A., ‘‘Degree of linear polarization in spectral radiances from water-viewing infrared radiometers,’’ *Appl. Optics*, vol. 38, no. 15, pp. 3157-3165, 1999.

Smith, W. L., R. O. Knuteson, H. E. Revercomb, W. Feltz, H. B. Howell, W. P. Menzel, N. R. Nalli, O. Brown, J. Brown, P. Minnett, and W. Mckeown, ‘‘Observations of the infrared radiative properties of the ocean - implications for the measurement of sea surface temperature via satellite remote sensing,’’ *Bull. Amer. Meteorol. Soc.*, vol. 77, no. 1, pp. 41-51, 1996.

Snyder, W., Z. Wan, Y. Zhang, and Y.-Z. Feng, ‘‘Requirements for satellite land surface temperature validation using a silt playa,’’ *Remote Sens. Environ.*, vol. 61, no. 2, pp. 279-289, 1997a.

Wan, Z. and J. Dozier, ‘‘A generalized split-window algorithm for retrieving land-surface temperature from space,’’ *IEEE Trans. Geosci. Remote Sens.*, vol. 34, no. 4, pp. 892-905, 1996.

Wan, Z. and Z.-L. Li, ‘‘A physics-based algorithm for retrieving land-surface emissivity and temperature from EOS/MODIS data,’’ *IEEE Trans. Geosci. Remote Sens.*, vol. 35, no. 4, pp. 980-996, 1997.

Wan, Z., Y. Zhang, X. Ma, M. D. King, J. S. Myers, and X. Li, ‘‘Vicarious calibration of the Moderate-Resolution Imaging Spectroradiometer Airborn Simulator thermal infrared channels,’’ *Appl. Optics*, vol. 38, no. 20, pp. 6294-6306, 1999.

TABLE I. Spatial analysis of MODIS TIR band brightness temperatures over a sub-area of 10 by 5 pixels in a lake in Kamchatka, Russia, on 13 April 2000, in terms of maximum temperature difference ΔT_b and standard deviation δT_b.

band	29	30	31	32	33	34	35	36
channel no. skipped								
number of pixels	50	50	50	50	50	50	50	50
ΔT_b (K)	0.44	1.22	0.24	0.50	1.32	2.48	1.96	2.18
δT_b (K)	0.11	0.26	0.04	0.12	0.52	0.68	0.43	0.47
specified NEΔT (K)	0.05	0.25	0.05	0.05	0.25	0.25	0.25	0.35

band	20	21	22	23	24	25	27	28
channel no. skipped								
number of pixels	50	50	50	50	50	50	50	50
ΔT_b (K)	1.10	81.2	8.60	0.66	33.4	1.34	1.10	0.48
δT_b (K)	0.31	17.5	1.67	0.16	4.07	0.35	0.28	0.10

band	20	21	22	23	24	25	27	28
channel no. skipped		9	4		9			
number of pixels	50	45	45	50	45	50	50	50
ΔT_b (K)	1.10	7.70	0.70	0.66	1.94	1.34	1.10	0.48
δT_b (K)	0.31	1.56	0.18	0.16	0.53	0.35	0.28	0.10
specified NEΔT (K)	0.05	(2.0)	0.07	0.07	0.25	0.25	0.25	0.35

TABLE II. Comparison between MODIS TIR band brightness temperatures and the calculated values based on in-situ measurement data around 16.247° S and 68.723° W in Lake Titicaca, Bolivia, on 15 June 2000.

band	15:26:20 UTC, 6/15/2000 calculated T_b (K) based on T_s=284.79K, θ_v=34.3°	MODIS T_b (K)	δT_b (K)	δT_b (K) from 6/14 night	std dev. δT_b (K)	δT_b (K) for radiometric accuracies specified at 1%	2%
20	283.50	284.13	0.63	0.26	0.31	0.21	0.42
21	282.98	284.11	1.13		1.56	(2.0K at 9%)	
22	283.03	283.28	0.25		0.18	0.22	0.44
23	281.74	281.90	0.16		0.16	0.22	0.44
24	254.17	253.42	-0.75		0.53	0.20	0.40
25	267.27	269.03	1.76		0.35	0.22	0.45
27	252.34	250.74	-1.60		0.28	0.30	0.59
28	265.52	265.72	0.20		0.10	0.36	0.71
29	282.02	282.23	0.21	-0.32	0.11	0.47	0.93
30	264.66	265.42	0.76		0.26	0.47	0.94
31	283.66	283.88	0.22	-0.09	0.04	0.61	1.21
32	283.36	283.24	-0.12		0.12	0.66	1.32
33	266.72	267.34	0.62		0.52	0.65	1.29
34	256.23	255.60	-0.63		0.68	0.61	1.22
35	247.27	247.26	-0.01		0.43	0.58	1.16
36	232.87	227.74	-5.13		0.47	0.53	1.05

TABLE III. Sensitivities of the calculated MODIS TIR band brightness temperatures on the uncertainties in measured atmospheric and surface data, and the comparison between their root sum squares (RSS) and the δT_b(K) values required for radiometric accuracies at 1% and 2%.

band no.	center wavelength (μm)	δT_a 0.5 (K)	δwv 10%	δCO_2 10 ppm	δO_3 -6%	surface BRDF	δT_s 0.25 (K)	RSS (K)	δT_b(K) required for radiometric accuracy 1%	2%
20	3.750	0.02	0.02			-0.02	0.23	0.23	0.21	0.42
22	3.959	0.02				-0.01	0.24	0.24	0.22	0.44
23	4.059	0.04		-0.01		-0.04	0.23	0.24	0.22	0.44
24	4.465	0.26		-0.10		-0.11	0.08	0.31	0.20	0.40
25	4.515	0.16	0.01	-0.01	0.01	-0.13	0.15	0.26	0.22	0.45
27	6.715	0.48	0.69			-0.01		0.84	0.30	0.59
28	7.925	0.37	0.47			-0.09	0.04	0.71	0.36	0.71
29	8.550	0.04	0.05		0.01	-0.07	0.23	0.25	0.47	0.93
30	9.730	0.18	0.01		0.55	-0.08	0.16	0.60	0.47	0.94
31	11.03	0.02	0.03			-0.02	0.24	0.24	0.61	1.21
32	12.02	0.02	0.04			-0.05	0.24	0.25	0.66	1.32
33	13.335	0.17	0.04	-0.19	0.04	-0.53	0.15	0.61	0.65	1.29
34	13.635	0.27	0.02	-0.28	0.03	-0.50	0.07	0.64	0.61	1.22
35	13.935	0.33	0.01	-0.26	0.04	-0.33	0.04	0.54	0.58	1.16
36	14.235	0.40	0.01	-0.27		-0.07	0.01	0.49	0.53	1.05

Note: zero values are not shown in the blank spaces for clarity.

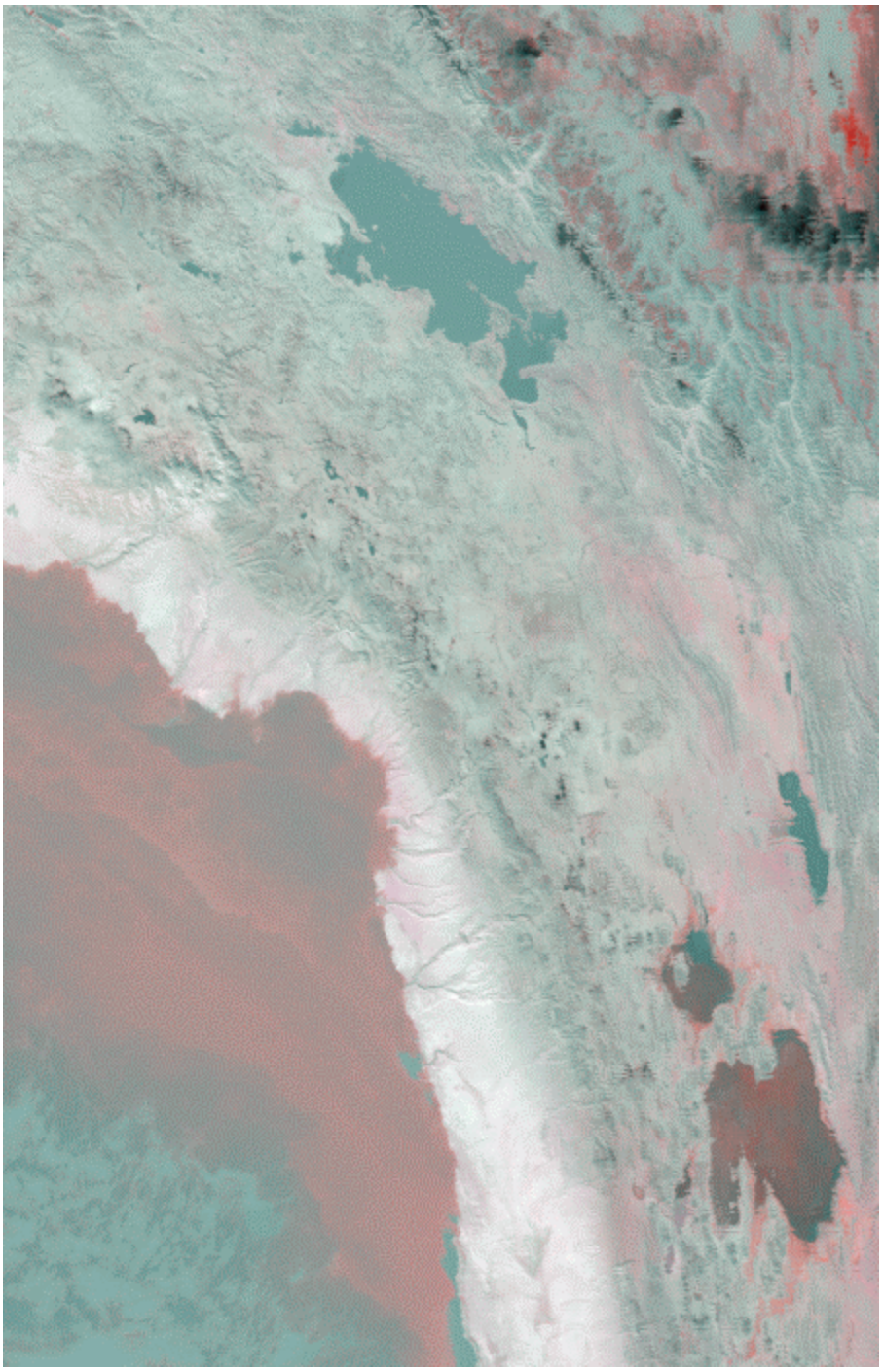

Fig. 1, black-white copy of a MODIS color composite image over Bolivia on 15 June 2000

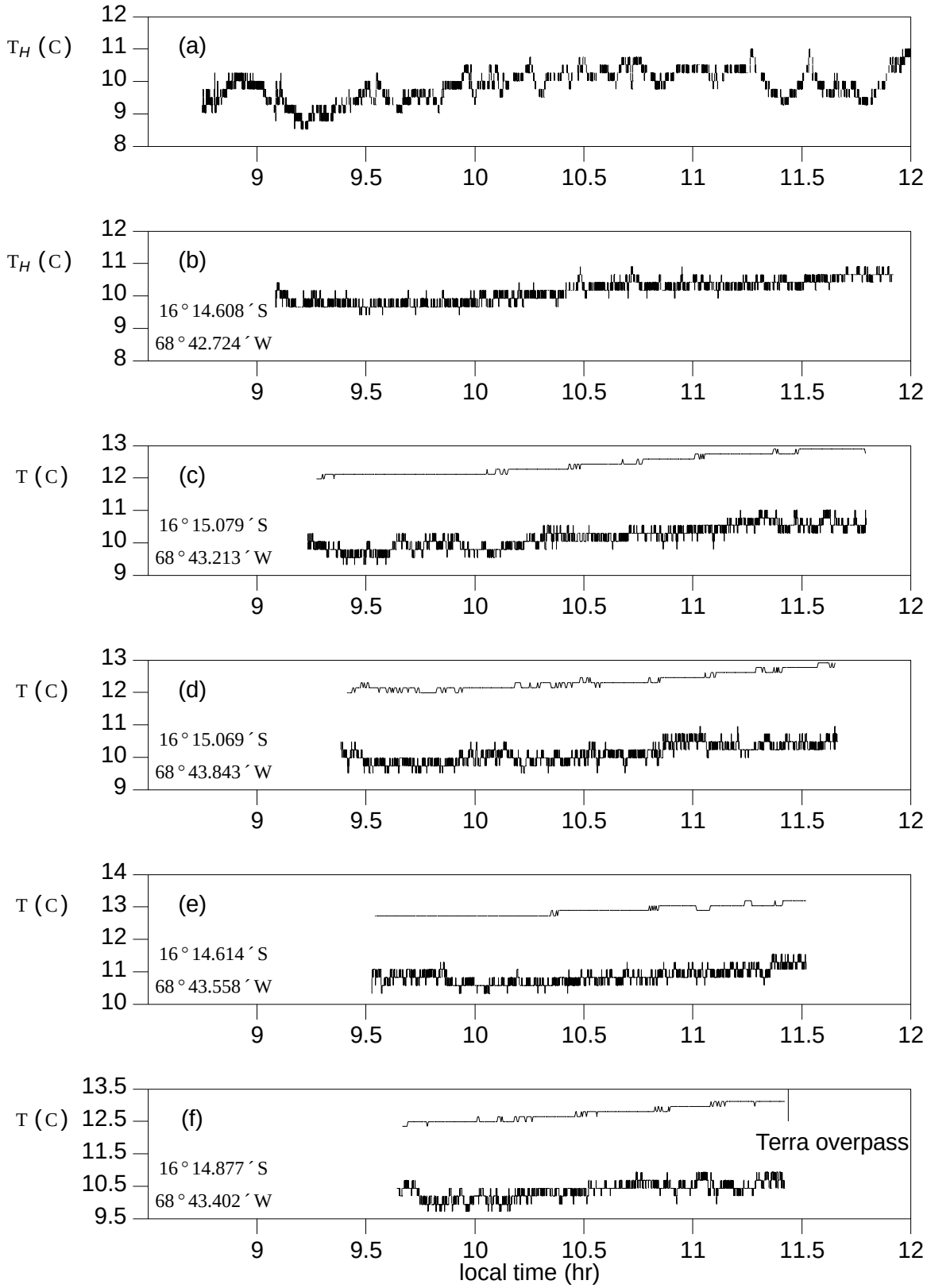

Fig. 2, Lake surface temperatures measured with an IR radiometer carried by boat (a), IR radiometers and thermistors by floating systems (b-f) at buoy positions.

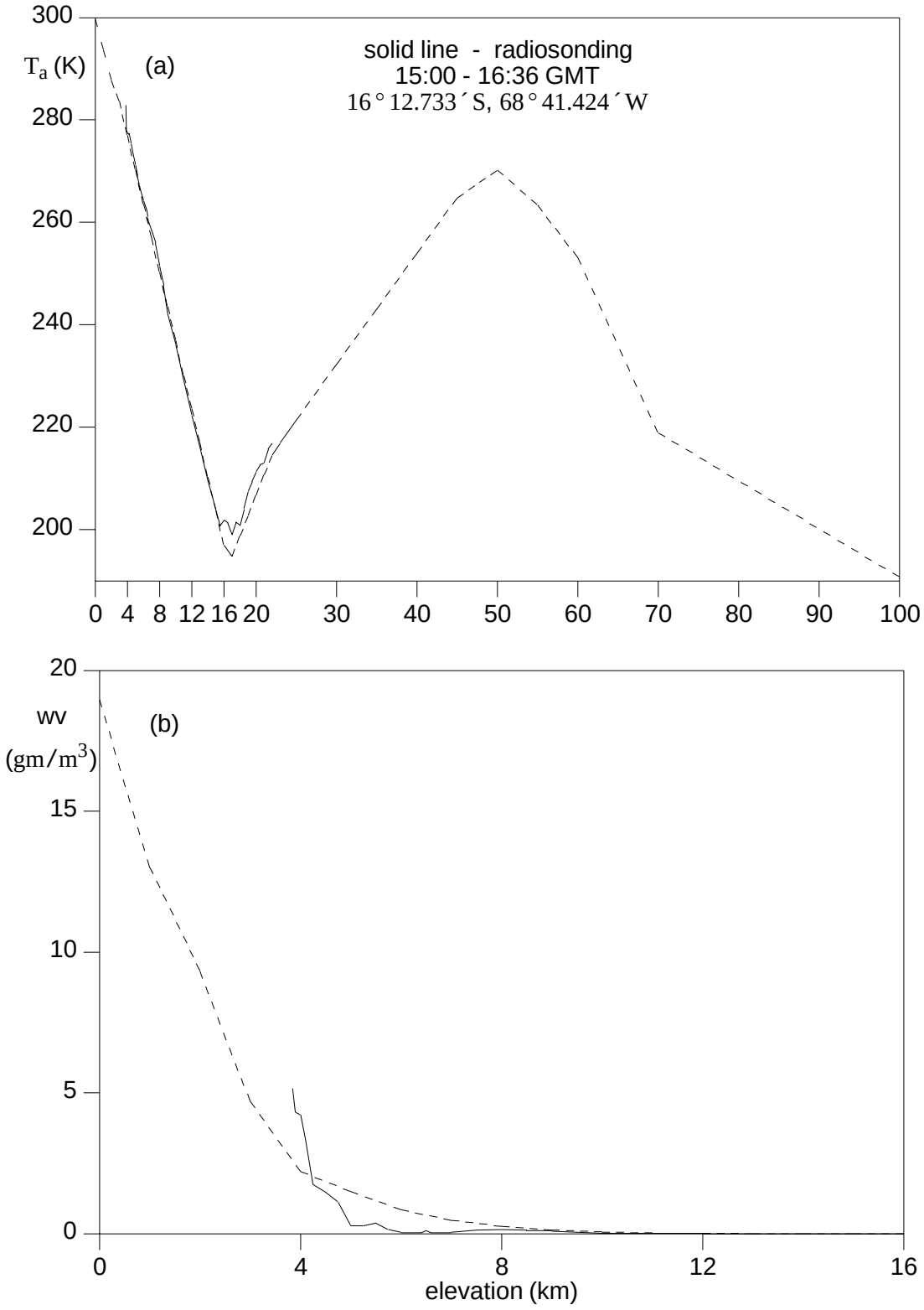

Fig. 3, Atmospheric temperature (a) and water vapor (b) profiles measured at Lake Titicaca, Bolivia on 15 June 2000 (solid lines), and the average tropical atmospheric profiles (dashed lines).

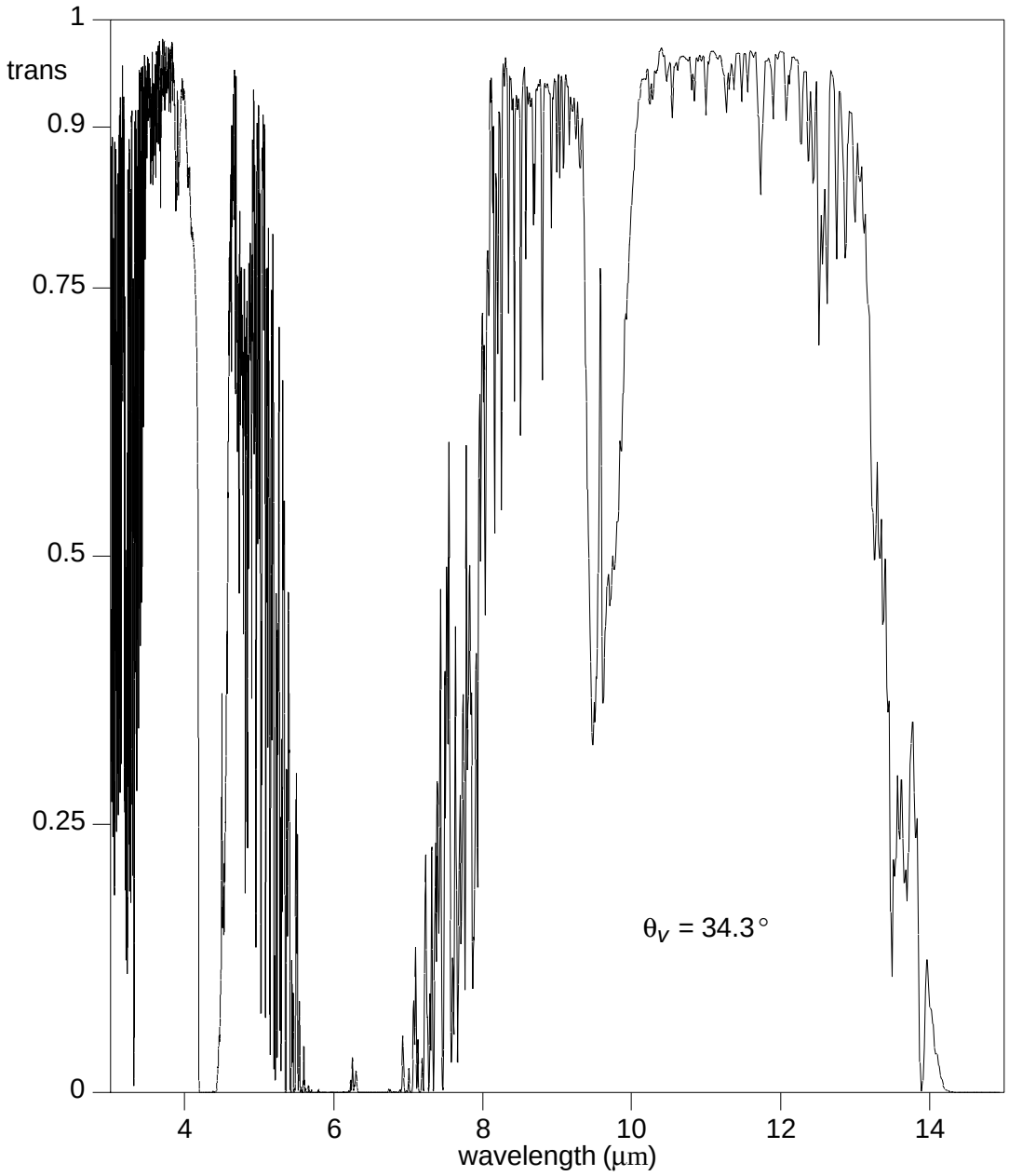

Fig. 4, Atmospheric transmission over Lake Titicaca, Bolivia, on 15 June 2000.